Oil & Gas Science and Technology - Rev. IFP Energies nouvelles **74**, 39 (2019)

https://doi.org/10.2516/ogst/2019007

Available online at:
ogst.ifpenergiesnouvelles.fr

REGULAR ARTICLE OPEN ACCESS

A Complete experimental study of oil/water interfacial properties in the presence of TiO_2 nanoparticles and different ions

Ali Khalilnezhad[1], Hosein Rezvani[2], Parastoo Ganji[3], and Yousef Kazemzadeh[4,*]

[1] Department of Petroleum and Natural Gas Engineering, Sahand University of Technology, Tabriz, Iran
[2] Department of Mining Engineering, Isfahan University of Technology, Isfahan, Iran
[3] Department of Petroleum Engineering, Science and Research Branch, Islamic Azad University, Fars, Iran
[4] Department of Petroleum Engineering, Amirkabir University of Technology, Tehran Polytechnic, Tehran, Iran

Received: 9 October 2018 / Accepted: 5 February 2019

Abstract. Previous studies on Nanoparticles (NPs) application for Enhanced Oil Recovery (EOR) methods have revealed their effective role in the rock wettability alteration, relative Interfacial Tension (IFT) and oil viscosity reduction, formation and stabilization of the emulsions, and reduced asphaltene precipitation, which are all in direct relationship with oil/water interfacial properties. This study focuses on the interfacial properties of oil/water in the presence of Titania NPs and different ions at different pressures and temperatures. For this, different concentrations of TiO_2 NPs in the Formation Water (FW) were prepared to monitor the effects of NPs on the oil/water IFT, carbonate rock wettability, zeta potential, and asphaltene adsorption. The results on IFT values indicated that NPs behavior at high pressures and temperatures is completely different, as compared to the ambient conditions, and 1000 ppm NPs introduced the lowest IFT at 600 psi and 60 °C. This reduction is potentially attributed to the asphaltene adsorption at the oil/water interface by TiO_2 NPs, which hinders the asphaltene deposition at the interface and in turn IFT increasing. Contact angle results revealed two distinctive behaviors for NPs at high and low concentrations. In other words, with the first interval (below the optimum concentration), an increase in NPs concentration led to a quick wettability alteration toward the water-wet condition, and with the second one (above the optimum concentration), there was an increase in contact angle with an increase in NPs concentration, which is due to the NPs stacking near the rock surface. These results were in good accordance with zeta potential measurements, in which 1000 ppm nanofluid presented the highest stability (zeta potential value of −46.9 mV). Batch adsorption experiments resulted that catalytic TiO_2 NPs are capable of adsorbing asphaltene at the oil/water interface. In addition, the results on fitting experimental data to the Langmuir and Freundlich Isotherms showed that the adsorption best fitted Langmuir Isotherm and hence the adsorption type is a monolayer.

Nomenclature

Acronyms

APS	Average Particle Size
CCD	Charge Coupled Device
DW	Distilled Water
EOR	Enhanced Oil Recovery
FW	Formation Water
HP–HT	High Pressure–High Temperature
IFT	Interfacial Tension
NPs	Nanoparticles
Rpm	Revolution Per Minute
SSA	Specific Surface Area
TDS	Total Disolved Solid
TH	Total Hardness

1 Introduction

NPs improve the reservoir geomechanical characteristics by modifying reservoir EOR mechanisms, which can finally help with an increase in the oil recovery [1, 2]. The Nano-formulations of polymers, surfactants, and colloidal dispersion gels could be embedded in this category. For instance, NPs can help with controlling the recovery processes, which are inconsistent with current and/or past technologies. Moreover, it has been seen that the viscosity of water, carbon dioxide, and surfactant solutions are usually lower than that of oil, therefore, adding NPs can adjust the injected

* Corresponding author: yusefkazemzade@yahoo.com

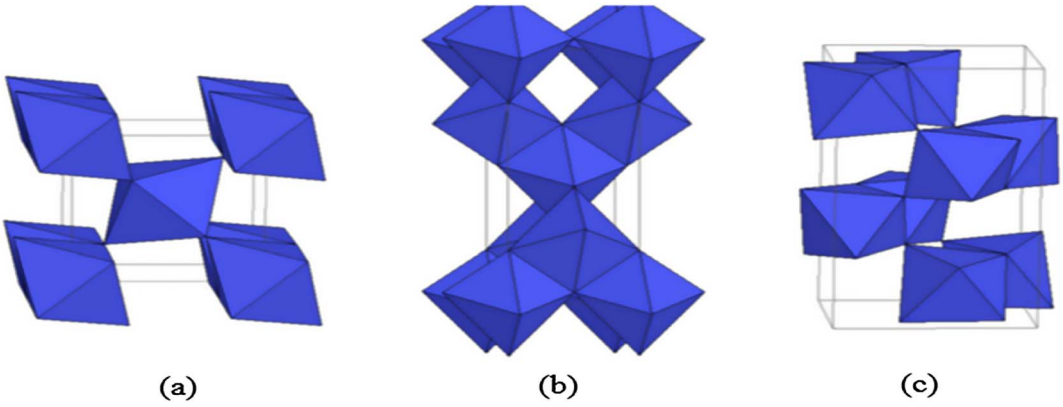

Fig. 1. Different crystalline phases of TiO_2 NPs: (a) Rutile, (b) Anatase, and (c) Brookite [17].

fluid viscosity at the optimum point [3]. As a consequence, an improvement in fluid transport and oil recovery can be achieved [4]. However, the adsorption of NPs onto the rock surface during movement in the pore throats can be harmful or beneficial to the Enhanced Oil Recovery, depending on specific conditions [5, 6].

Some NPs are capable of adsorbing asphaltene particles present in the crude oil [7–12]. This would prevent IFT increase, asphaltene precipitation and deposition, and wettability alteration toward the oil-wet condition. Catalytic NPs including NiO, Fe_3O_4, TiO_2, CuO, Al_2O_3, etc. are mostly categorized in this group [5, 13]. The adsorption process is mainly controlled by various factors:

- Type of adsorbent and its properties

Both physical and chemical properties of the adsorbent affect the adsorption process. Chemical properties involve various types of functional groups available on the adsorbent surface. Ionization of adsorbent surface also affects the adsorbent properties. Since adsorbents could differ in shape (*i.e.* powder or grain), physical properties of adsorbent, including specific surface area and pore distribution play an important role. Adsorbents usually present large surface pores and have grains appearing in spherical or irregular shapes. The smaller particles of the adsorbent, the faster they get in contact with the fluid phase.

- Adsorbate

The chemical properties of adsorbate are important in the adsorption process. The size of adsorbed molecules controls the adsorption rate. The bigger molecules have a lower solubility in the fluid and tend to leave the medium and adsorb onto the adsorbent more quickly. On the other hand, bigger molecules occupy larger areas when adsorbing onto the adsorbent. Therefore, smaller molecules are sometimes beneficial. The shape of molecules also affects the solubility. The solubility of adsorbate plays a key role in controlling the adsorption equilibrium. The effect of solubility on the adsorption process is based on the binding between the adsorbent and solvent. The stronger than binding, the weaker than adsorption.

- Temperature

Temperature applies two main effects to the adsorption process: on the one hand, an increase in temperature decreases the diffusion rate of adsorbate molecules into the external layers and inside the adsorbent pores. As a result, the viscosity of the solution reduces. On the other hand, the effect of temperature on the adsorption process provides some useful information on enthalpy and entropy changes during adsorption. An increase in temperature leads to the increase in the adsorption rate before the solution reaches the equilibrium. Generally, temperature elevation amplifies the movement of the molecules on the surface and impedes the formation of a monolayer on the surface. Therefore, the adsorption would become slower and repulsion results in the less surface coating. In another word, since the adsorption phenomenon is an exothermic process, adsorption would be more intense at lower temperatures. At higher temperatures, the adsorption rate increases, whereas the total adsorption capability decreases.

- pH of solution

Hydrogen ions and hydroxyl groups present in the medium are strongly adsorbed; therefore, the adsorption of the other ions is mainly affected by the pH of the solution. Acid/base ionization is also effective in the adsorption process, which itself is dependent on the pH. The adsorption mainly increases with a decrease in pH. However, it should be noted that the effect of temperature and pH generally depends on the type of adsorbent and for each adsorbent, there is an optimum temperature and pH.

Titanium dioxide (TiO_2) NPs, also known as titanium (IV) oxide or Titania NPs, hold all the properties of titanium dioxide with the difference that their smaller size makes them more efficient, which is due to the increased surface area of NPs. The photocatalytic activity of Titania improves as the particle dimensions reduce to the nanoscale, which results from the increased specific surface area [14]. These NPs are very chemically stable, cost-effective substance. There are three different crystalline phases of Titanium dioxide, namely: Rutile, Anatase, and Brookite (Fig. 1). Rutile is the most stable phase and the other

Table 1. SARA analysis of the crude oil.

Compositional analysis of the crude oil											
Type	C_1	C_2	C_3	i-C_4	n-C_4	i-C_5	n-C_5	C_6	C_{7+}	H_2S	CO_2
Mole %	47.66	11.32	6.48	1.08	2.89	1.21	1.49	2.38	25.49	0	0

SARA analysis				
Type	Saturate	Asphaltene	Resin	Aromatic
Wt.%	51.35	8.59	9.78	30.28

two phases are converted to Rutile by temperature elevation. Rutile and Anatase phases are spatially tetragonal, while Brookite has an orthorhombic form [15, 16].

In the EOR processes, the addition of TiO_2 NPs to the injected fluid is capable of altering rock wettability and preventing asphaltene precipitation [18]. However, it has been reported that exceeding the optimum concentration does not necessarily improve the situation. Sometimes, it even results in NPs aggregation and their subsequent movement from the bulk phase toward the oil/water interface. As a result, the interface gets stronger and the IFT between two fluids rises [19, 20].

There is a vast amount of literature on the experimental investigation of NPs for EOR methods [6, 21–24]. Haroun *et al.* compared the injection of smart water and nanofluids. They concluded that the addition of suitable NPs to the injected water can improve the recovery factor from 46–63% to 57–85% [25]. In their analysis of ZnO NPs, Moghadam and Azizian analyzed the effect of these NPs on anionic surfactants at the fluid/fluid interface. They reported a decreased oil/surfactant IFT with the addition of NPs [26]. In a major attempt in 2016, Kazemzadeh and coworkers surveyed the asphaltene precipitation in the oil phase by IFT measurements. They announced that Fe_3O_4 NPs are able to prevent asphaltene precipitation at the oil/water interface by adsorbing large asphaltene particles. They also observed a considerable IFT reduction between oil and water in the presence of NPs [9]. Castillo *et al.* proved that the size of adsorbents and their shape could influence the adsorption process. They observed great variances in interactions between adsorbed asphaltene with macro surfaces and NPs [27]. In another study, Franco-Aguirre *et al.* used SiO_2 NPs with an anionic surfactant to alter the wettability of sandstone in gas-condensate reservoirs. They observed that the contact angle changed from 0° to 118° for water/rock/air system [28]. Rezvani *et al.* synthesized Chitosan-coated Fe_3O_4 nanocomposites to investigate their possible EOR effects. Based on their sand pack flooding, they observed an additional oil recovery factor of 10.8% with the addition of the synthesized nanocomposite to the seawater in the tertiary mode, which resulted in the ultimate recovery factor of 67.5%. They attributed this improvement to the decrease in oil/water IFT, prevention of asphaltene precipitation, the emulsion formation, and rock wettability alteration [7].

The current research presents a complete study of the oil/water interfacial properties in the presence of TiO_2 NPs for the first time. The IFT measurements were carried out at different pressures and temperatures in the presence and absence of NPs and the optimum concentration of NPs was determined. The same concentrations of nanofluids were also selected for contact angle measurements to determine the optimum concentration. Thereafter, the stability of NPs in the FW was analyzed by zeta potential measurements and thus compared with the results of IFTs and contact angles. Finally, the asphaltene adsorption by TiO_2 NPs was analyzed by batch adsorption experiments.

Table 2. Analytical experiments performed on FW.

Experiments	Amount	Unit
Cl^-	93 056	ppm
Na^+	98 450	
K^+	23 000	
Fe^{3-}	0.07	
POu^{3-}	0.17	
SO_4^{2-}	1200	
Ca^{2+}	3800	
Mg^{2+}	1944	
Total salinity	221 450.24	
Total hardness (TH)	17 500	
pH	7.01	–
Turbidity	0.4	NTU
Density at 20 °C	1.1005	g/cm^3
Conductivity	184 100	µs/cm

2 Materials and methods

2.1 Materials

2.1.1 Crude oil, formation water, and carbonate rock

The crude oil and Formation Water (FW) used in this research were obtained from one of the Iranian oil reservoirs. The crude oil had a gravity of 31.5 °API. The results of SARA (Saturate, Aromatic, Resin and Asphaltene) and compositional analyses are presented in Table 1.

The compositional analysis of FW is tabulated in Table 2. The total salinity was measured as 221 450 ppm. Moreover, the surface outcrop of the reservoir formation

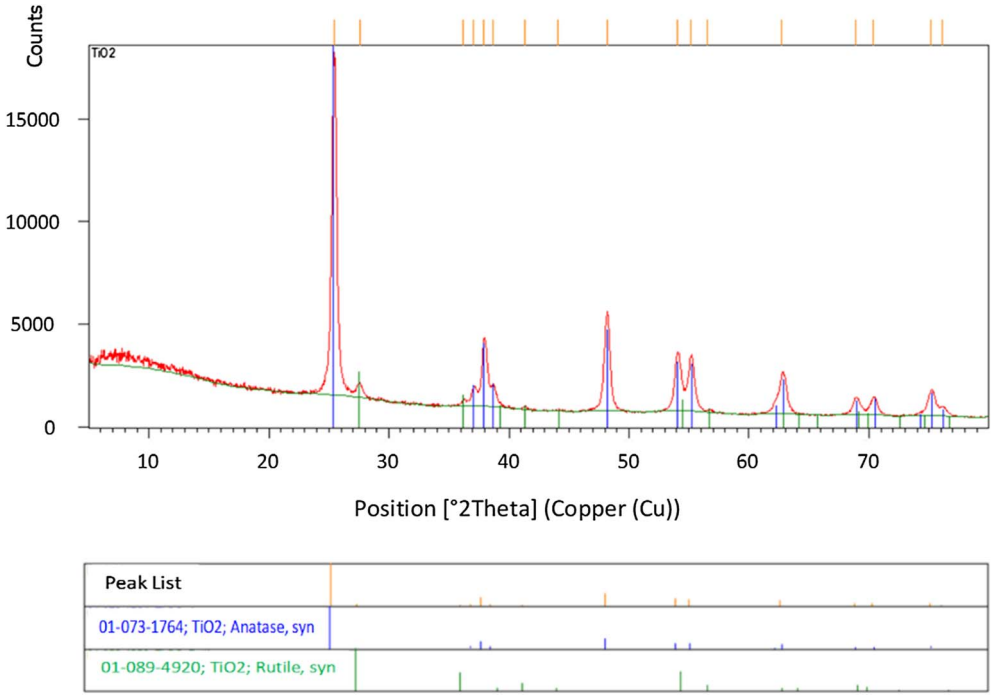

Fig. 2. XRD pattern of TiO_2 NPs provided by *US Research Nanomaterials Inc.*

was trimmed into thin sections for evaluation of wettability alteration.

2.1.2 TiO_2 nanofluids

The solid Anatase/Rutile TiO_2 nanopowders were purchased from the *US Research Nanomaterials Inc.* and used as received. The XRD and SEM of these NPs are shown in Figures 2 and 3, respectively. Further detailed properties of NPs are presented in Table 3.

The nanofluid preparation process included the addition of NPs to the FW, which was followed by the ultrasonication process for 30 min with the power of 300 W. The apparatus used was the Ultrasonic Probe DA UP-400 (*Development of Ultrasonic Technology Co., Iran*). To prevent NPs from aggregation during sonicating process, the ultrasonication was performed in an ice bath to prevent temperature elevation of the nanofluid. This process was similarly repeated before all the following experiments.

2.2 Methods

2.2.1 Interfacial tension measurement

The pendant drop IFT–400 apparatus manufactured by *Fars EOR Technology* (Fig. 4) was utilized to investigate the effect of TiO_2 NPs on IFT values under reservoir conditions (*i.e.* high pressures and temperatures). The apparatus supported measuring from 1–72 mN m^{-1} with an accuracy of 0.1 mN m^{-1}. The pressure and temperature accuracy of the device was 0.5% full scale and 0.1 °C, respectively. The camera used in this device was a 2-megapixel CCD-HD camera consisting of a *C*-mount macro lens with

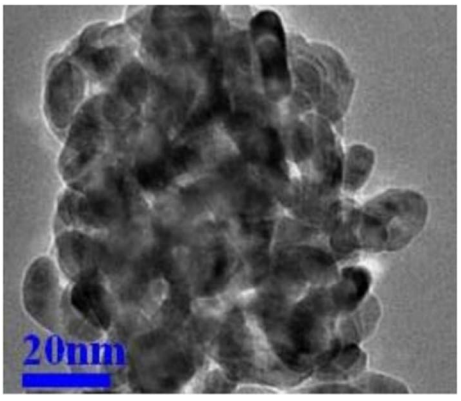

Fig. 3. SEM of TiO_2 NPs provided by *US Research Nanomaterials Inc.*

a magnification of ×10. The experiments were carried out at different temperatures (40, 60, and 80 °C) and pressures (14.7, 600, 1200, and 1800 psi) for six concentrations of NPs (250, 500, 750, 1000, 1500, and 2000 ppm) in FW, as presented in Table 4.

At each experiment, the pressure reduced to atmospheric pressure to compare the efficiency of NPs at atmospheric pressure (14.7 psi) with higher pressures. The equilibrium IFT at which the interfacial tension is stable was measured at each experiment.

2.2.2 Contact angle measurement

The inverted sessile drop method was adopted for analyzing the wettability alteration (Fig. 5). The apparatus used was

Table 3. Detail properties of TiO_2 NPs provided by *US Research Nanomaterials Inc.*

Composition (vol. %)		Purity (%)	APS (D50) (nm)	SSA (m^2/g)	Color	Bulk density (g/cc)	pH
Anatase	Rutile						
80	20	>99	20	10–45	White	0.46	5.5–6.0

*APS: Average Particle Size.

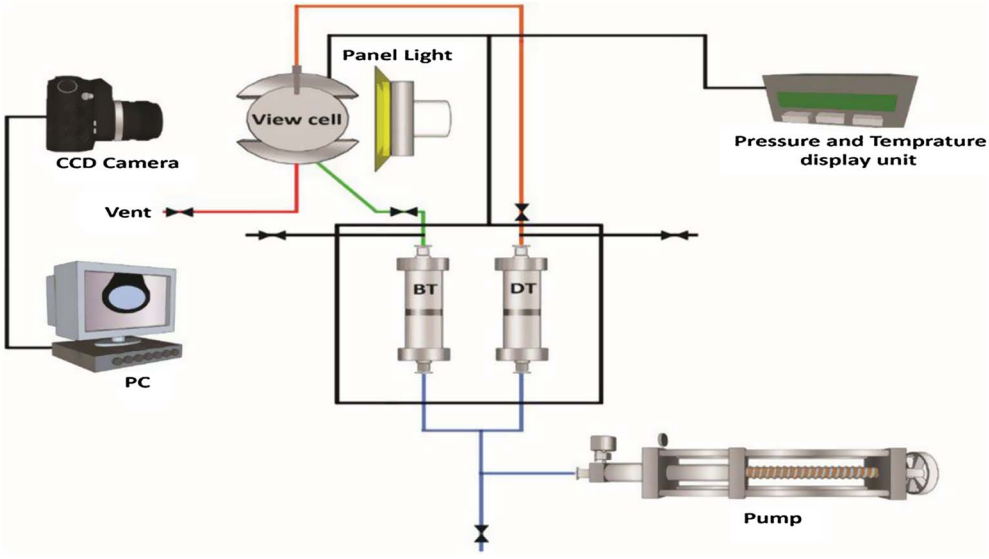

Fig. 4. Schematic view of HP–HT pendant drop IFT–400 apparatus.

manufactured by *Fars EOR Technology* and supported the measurements from 10 to 180° with an accuracy of ±3°.

Firstly, the rock slabs trimmed from reservoir outcrop were polished and washed with toluene to remove any possible impurities. Afterward, they were aged 3 days in FW to become completely water-wet. They were then aged in the reservoir's crude oil for 21 days at the temperature and pressure of 80 °C and 2500 psi, respectively [29]. The same six nanofluids (as used in IFT evaluation) were selected to evaluate the wettability alteration.

2.2.3 Zeta potential measurement

In order to investigate the effect of ions of FW and TiO_2 NPs on the surface electrical charges and in turn wettability alteration, different zeta potential measurements were conducted. Since the existence of clay minerals, including kaolinite, calcite, quartz, and other metallic components in reservoir rock is prevalent [31], the carbonate rock samples were first pulverized to <45 μm at 1354 rpm and 4 wt.% rock powder was added to different Titania nanofluids (500, 1000, and 2000 ppm) [32, 33]. To compare the results, the experiments were followed by measuring the zeta potentials of Distilled Water (DW) and FW + 4 wt. % rock powder. The apparatus used was Microtrac Zeta Check (USA) with a measuring range of –200 mV to +200 mV and an accuracy of ±1 mV.

Table 4. Experimental design for IFT measurement.

Number	Concentration of NPs in the FW (ppm)	Temperature (°C)	Pressure (psi)
1	250	80	1800
2	250	60	1200
3	250	40	600
4	500	80	1800
5	500	60	1200
6	500	40	600
7	750	80	1200
8	750	60	600
9	750	40	1800
10	1000	80	600
11	1000	60	1800
12	1000	40	1200
13	1500	80	1200
14	1500	60	600
15	1500	40	1800
16	2000	80	600
17	2000	60	1800
18	2000	40	1200

14.7

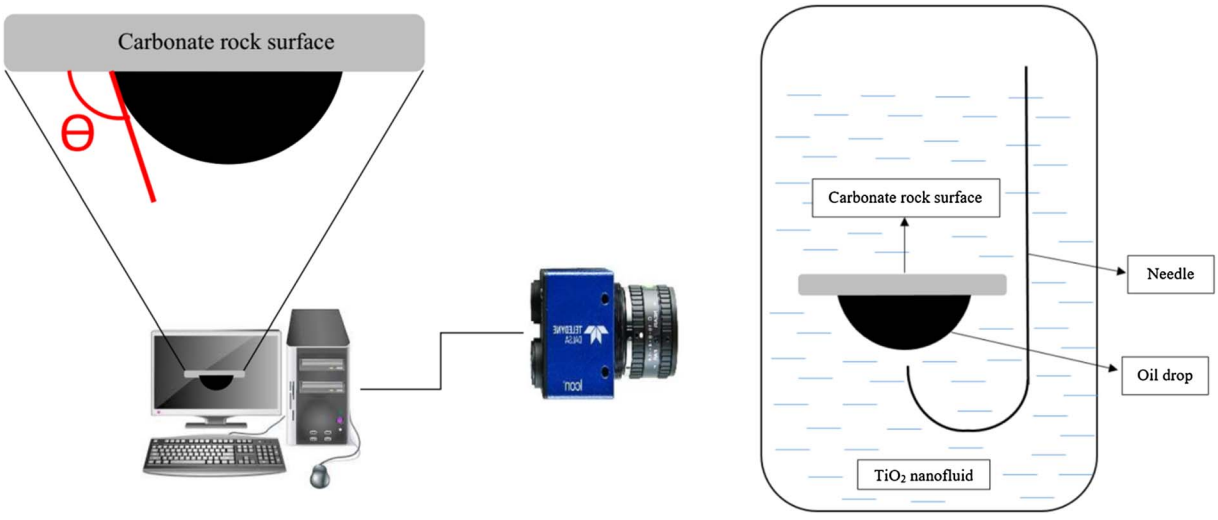

Fig. 5. The inverted sessile drop method used for wettability assessment [30].

2.2.4 Asphaltene adsorption analysis

There are several methods to evaluate the asphaltene adsorption by NPs like Thermogravimetric Analysis (TGA) and UV–Vis spectroscopy. In this research, the latter has been adopted to evaluate the asphaltene adsorption by TiO_2 NPs and their effect on the prevention of asphaltene precipitation. In order to analyze the amount of asphaltene adsorption by TiO_2 NPs, different batch adsorption experiments were carried out. The procedure was based on the method performed by previous authors [34, 35].

TiO_2 NPs used in this research were nonporous and held a specific surface area of 10–45 m^2/g. Asphaltene was extracted from the crude oil using the IP-143 standard and used in the preparation of the synthetic oil. The oil was synthesized with a toluene/*n*-heptane ratio of 60/40 vol% and 10–3000 mg/L asphaltene. The experiments included the addition of TiO_2 NPs to the synthetic oil with a TiO_2/oil ratio of 10:1 gr/L. The mixture was shaken at 400 rpm and then was aged to reach an equilibrium. Centrifugation was used to separate the asphaltene of the solutions at 5000 rpm. The asphaltene concentration in the supernatant was determined using Dynamica DB-20S UV/Visible Double Beam Spectrophotometer at 700 nm. The apparatus supported a full spectral scan from 190 to 1100 nm and a wavelength accuracy of 0.3 nm. The asphaltene adsorption by NPs was analyzed by monitoring the changes in the asphaltene concentration before and after combining the synthetic oil with NPs. The following equation calculates the amount of adsorbed asphaltene (eq. (1)):

$$q_t = \frac{C_0 - C_t}{m} V, \tag{1}$$

where q_t represents the adsorbed asphaltene (mg/g), C_0 is the initial asphaltene concentration (mg/L), C_t is the asphaltene concentration at time t (mg/L), m is the mass of solid particles (gr), and V stands for volume of solution (L).

3 Results and discussions

3.1 IFT measurements

3.1.1 Effect of ions present in FW

Based on the previous results, oil/water IFT linearly increases with an increase in pressure and decreases with an increase in temperature [36–39]. However, the presence of ions potentially alters the linear variation of IFT with pressure and temperature [30]. In this case, the IFT value is a function of temperature, pressure, salinity, total acid number, and asphaltene content. Therefore, the ultimate IFT value depends on the amount of surface active agents at the oil/water interface [40]. There are different reports regarding the effect of ions in the water on the oil/water IFT [41–43]. Generally, low ionic strength induces the salting-in effect in which potential-determining ions added to the water interact with crude oil components and a relative solubility of the oil components in the water phase occurs, as a result. This would decrease the oil/water IFT. However, some reports show that high ionic strength depletes the oil/water interface and makes the natural surfactant of the crude oil to move to the oil bulk. This is true even in the case of high potential-determining ions in the water [44].

The results on FW/oil IFT variations with pressure and temperature in the absence of TiO_2 NPs are demonstrated in Figure 6. As illustrated, the IFT between oil and FW ascends with an increase in pressure at all temperatures, which is mainly due to the high salinity of the FW and therefore the salting-out effect. However, with an increase in temperature, the possibility of hydration of potential-determining ions available in the FW (*i.e.* Ca^{2+}, Mg^{2+}, and SO_4^{2-}) becomes low, which is accompanied by an improvement in their coefficient activity. These two factors together are considered as the main reason for the decrease in IFT values at higher temperatures (*i.e.* 60 and 80 °C). Actually, the different trends of IFT with pressure at different

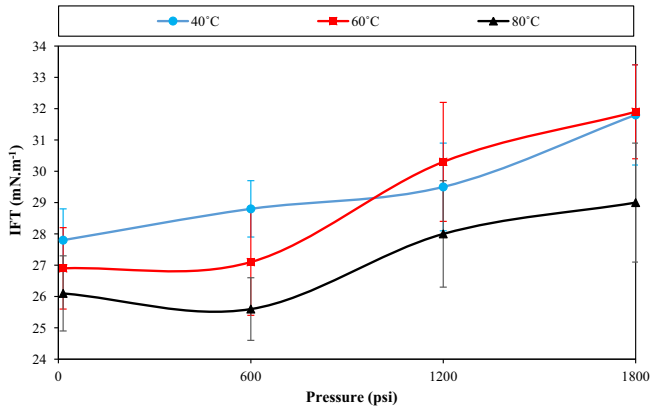

Fig. 6. The FW/oil IFT variations with pressure at different temperatures of 40, 60, and 80 °C.

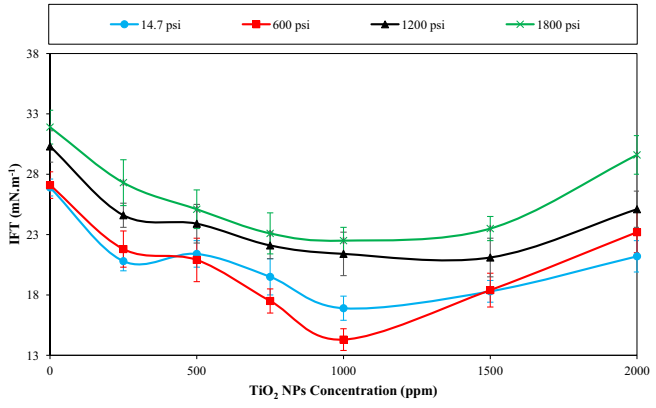

Fig. 7. IFT variations with TiO_2 NPs concentration for different pressures at 60 °C.

temperatures emanate from thermal cracking of large oil molecules at high temperatures.

3.1.2 Effect of TiO_2 NPs

Several surveys have revealed that NPs aggregation is amplified with temperature elevation due to the increased random motion of NPs in the base fluid, which in turn reduces the NPs efficiency [45–48]. However, an increasing number of studies have confirmed the role of some NPs in the reduction of the IFT between crude oil and water [2, 49–51]. Therefore, the efficiency of NPs at elevated temperature and pressure is a vital factor for practical application of nanofluids in the oil fields.

It is apparent from Figure 7 that the smallest value of IFT between crude oil and nanofluid has been observed for 1000 ppm Titania nanofluid at 600 psi and 60 °C. This concentration is regarded as the optimum concentration at all pressures. An increasing trend beyond the optimum concentration (1000 ppm) is also clear in Figure 7, which is mainly due to the increased NPs concentration and therefore augmented attractive forces between particles with increased charge density. This would ultimately increase the IFT values.

Pressure is a significant effect on IFT variations that is observed in Figure 7. Based on the experiments in this research, IFT variations are different at high and low pressures. From 14.7 up to 600 psi, the IFT values decrease as pressure increases. However, from 600 up to 1800 psi, an increase in pressure increases the IFT. With this in mind, the binary behavior of NPs at the optimum concentrations at different pressures results from intermolecular forces. In fact, at low pressures, asphaltene particles present in the crude oil drop tend to move to the oil/water interface. At this situation, NPs create a false surface that adsorbs large asphaltene particles and prevents the IFT increase, as compared to the case when NPs are absent in the system. Therefore, the intermolecular balance at the interface deducts the IFT between oil and FW. The high stability of NPs in the base fluid at low pressures results in more adsorption of asphaltene particles onto the surface of NPs, which prevents the asphaltene precipitation and controls the IFT values. On the other hand, at high pressures, the stability and therefore the efficiency of NPs in asphaltene adsorption reduces, which affects the IFT variations. Given these points, pressure and concentration of NPs in the base fluid are the fundamental parameters in NPs stability. It is also of great importance to imply that the stability reduces with an increase in pressure and NPs concentration; however, pressure increase stabilizes the asphaltene particles. As a result, the IFT reduction at optimum cases is intensified at low pressures.

Figure 8 indicates the IFT variations with pressure for different concentrations of NPs. As it is clear, the addition of TiO_2 NPs to FW intensifies the total rate of IFT increasing with pressure. It is observed that in the absence of NPs, the IFT increasing rate is 0.0031, whereas, the addition of 250, 1000, and 2000 ppm NPs to the base fluid rises IFT increasing rate to 0.00037, 0.004, and 0.0046, respectively. A relative decrease in IFT values with pressure at 1000 ppm is also observed. To that end, a deeper understanding of the relationship between IFT and temperature/pressure seems to be obligatory for the explanation of the NPs behavior at high pressures and temperatures. In fact, a compact arrangement of NPs due to the pressure lift intensifies the charge density. This would cause the NPs to move toward the interface and create a strong, rigid interface, which ultimately increases the oil/water IFT. Figure 8 confirms the significant impact of NPs on the rate of IFT increasing as the NPs concentration goes up, which is the likely reason for the low efficiency of NPs at high pressures.

Figure 9 depicts the IFT variations with TiO_2 NPs concentration at different temperatures. The figure clearly shows a decreasing IFT trend with the addition of TiO_2 NPs from 0 to 1000 ppm at all temperatures. It is also obvious that 1000 ppm is the optimum concentration of NPs at all temperatures. Beyond the optimum concentration, increasing NPs concentration increases the IFT values at all temperatures, which is mainly due to the high aggregation of NPs with an increase in concentration.

The catalytic behavior of TiO_2 NPs increases as temperature goes up, which can help to the improved thermal cracking of the large oil molecules and decreases the crude

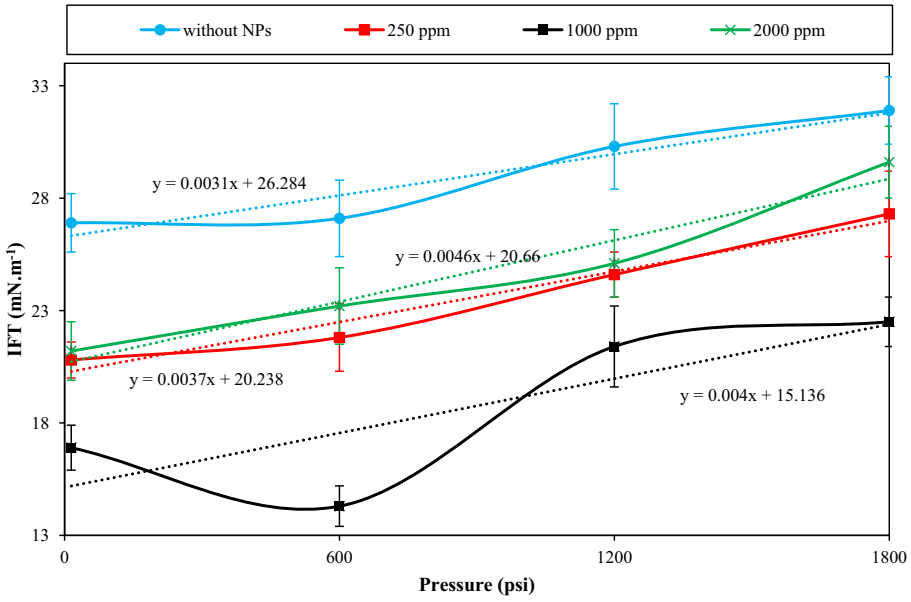

Fig. 8. IFT variations with pressure for different concentrations of TiO_2 NPs at 60 °C.

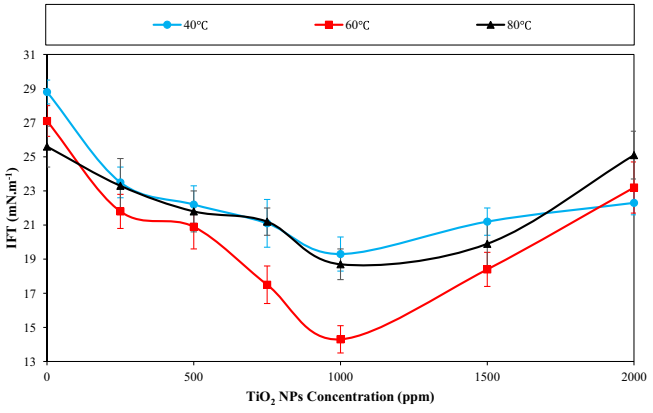

Fig. 9. IFT variations with TiO_2 NPs concentration for different temperatures of 40, 60, and 80 °C at 600 psi.

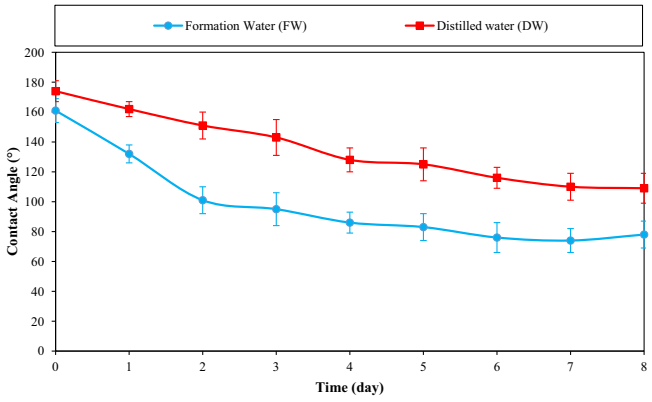

Fig. 10. FW and DW/crude oil/rock contact angle measurements with time.

oil viscosity [52]. This would reduce the oil/water IFT. On the other hand, the temperature elevation increases the Brownian motion of NPs in the suspension that intensifies the NPs collision together. Therefore, the stability of the nanofluid may decrease owing to the NPs aggregation. Brownian motion is also responsible for liquidification at the interface. This is responsible for improving oil/water IFT. Overall, temperature elevation has multilateral effects on the ultimate oil/water IFT and depending on the conditions, the oil/water IFT may increase, decrease or does not change considerably.

3.2 Contact angle measurements

3.2.1 Effect of ions present in FW

Fine migration, rock mineral dissolution, Multicomponent Ion Exchange (MIE), alteration of surface electrical potential, Electrical Double Layer expansion (EDL), dolomitization, and pH alteration are among the well-known EOR mechanisms have been reported for injection of saline water into the oil reservoirs [53]. Potential-determining ions present in FW play a key role in the alteration of rock wettability. Previous reports have shown that even a small amount of SO_4^{2-} ions in comparison with inactive ions of FW can alter the rock wettability [44, 53].

The dynamic contact angle measurements of FW/rock/oil and DW/rock/oil systems are shown in Figure 10. The DW/oil/rock contact angle was calculated as 174°. The results show that present ions in the FW bring an additional reduction of 13° in contact angle at the first moment. A relatively good wettability alteration after 7-day treatment by FW (from 161° to 74°) is also observed in the figure. However, a relative increase on the 8th day of treatment is observed. In fact, high saline FW is prone to the salting-out effect, in which high concentrations of ions at

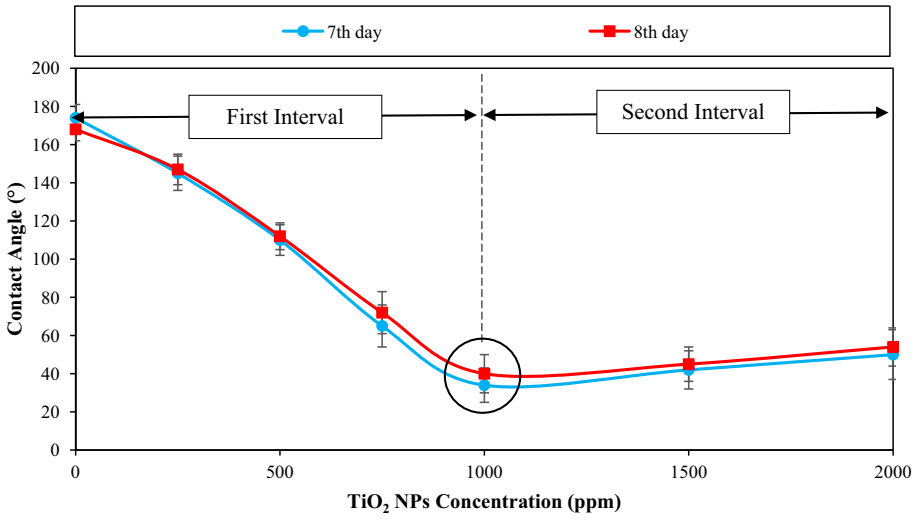

Fig. 11. Contact angle measurements for different concentrations of TiO_2 NPs after a 7 and 8-day treatment at ambient conditions.

the interface deplete the interface from natural surfactants and makes them move to the oil bulk or solid/oil interface. This would increase the oil-wet wettability of the rock as time goes on. In addition, inactive ions present in the FW including Na^+, Cl^-, HCO_3^-, etc. prevent approaching of potential-determining ions to the rock surface, and hence, reduce the efficiency of active ions [44]. All in all, based on the results, it is clear to mention that wettability alteration by FW is not enough and further irreversible wettability improvement by the addition of NPs seems to be essential.

3.2.2 Effect of TiO_2 NPs

Figure 11 depicts the contact angle variations with NPs concentration after a 7 and 8-day treatment. As it is clear, two distinctive intervals can be observed for contact angle results. At low concentrations (first interval), the reduction of contact angles occurs with a steep slope. As indicated, a reduction of 140° (from 174 to 34°) is observed on the 7th day of treatment, which implies a strong wettability alteration from oil-wet to a water-wet condition. On the contrary, at high concentrations (second interval), an increase in contact angle happens due to the increase in NPs concentrations. The increasing slope of the contact angle with the second interval is considerably smaller than the reduction rate with the first interval. Therefore, it all boils down to the fact that the NPs behavior in the FW is different at the two intervals.

Figure 12 illustrates the impact of an increase in NPs concentration on the disjoining pressure and in turn wettability alteration. As shown, increasing NPs concentration induces a compact arrangement of NPs in the wedge layer. This implies an increased number of NPs in the volume unit, which applies a high disjoining pressure to the surface against adhesion force between crude oil droplet and rock surface. As a result, the crude oil droplet gradually desorbs from the rock surface and NPs can attach to the surface and, as a result, the rock wettability changes.

Foremost, a subtle understanding of disjoining pressure seems to be necessary. It is by definition the required pressure for overcoming the oil adhesion force to the solid's surface to detach the oil from the surface. It is actually the pressure difference between the phase bulk and thin film adjacent to the rock surface, which can be considered as an EOR mechanism for NPs. In this mechanism, NPs create a wedge film with discontinuous fluid on the surface. Brownian motion and electrostatic repulsive forces between NPs are the key factors for developing this mechanism.

As the size of NPs decreases and as the concentration of NPs increases, the repulsive forces get stronger. This arrangement of NPs in the wedge layer inserts higher pressure on the fluid/solid interface. The more the number of NPs in the unit of volume, the stronger the pressure inserted in the interface. Surprisingly, this pressure can sometimes reach up to 50 000 psi. It is worth noting that with the exertion of such forces upon the interface, an oil displacement occurs to reach a balanced condition. Taken together, like in other colloidal systems, particle size, temperature, the salinity of carrier fluid, and properties of available phases all affect the intensity of disjoining pressure.

As noted earlier, NPs accumulation near the rock surface detaches the oil droplet from the surface. Thereupon, NPs adsorb onto the rock surface and reduce the contact angle. This reduction of the contact angle is continuous until reaching the optimum concentration. At the optimum concentration, the highest wettability alteration occurs, as shown in Figure 12. Beyond this concentration, NPs stack in a laminated structure near the rock surface, which no longer affects the wettability. The adsorption of NPs onto the rock surface increases with an increase in NPs concentration. However, at high concentrations (second interval), the added NPs adsorb onto the surface of the attached NPs to the rock surface. The resulting stack of NPs without any contact with the rock surface is no longer able to further reduce the contact angle and hence alter the wettability condition (Fig. 13). That is to say, the optimum concentration is the most efficient and

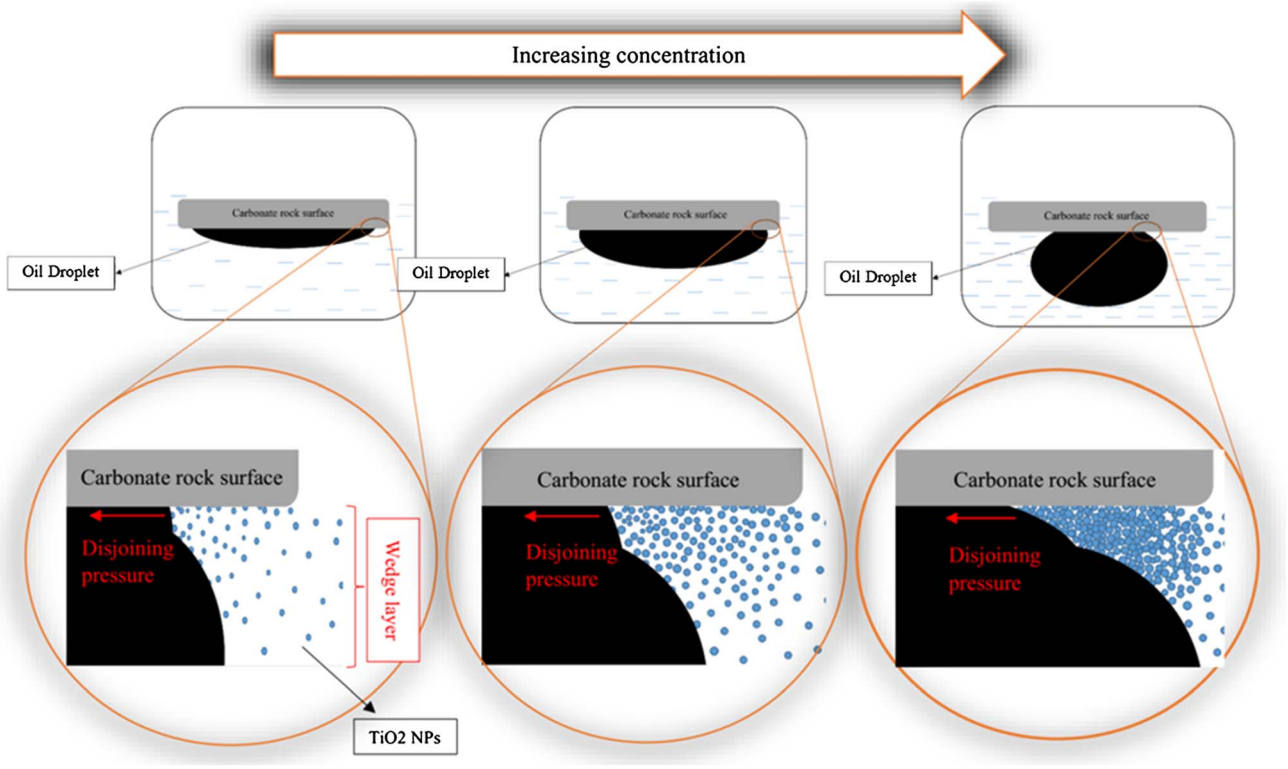

Fig. 12. Wettability alteration with increasing NPs concentration [5].

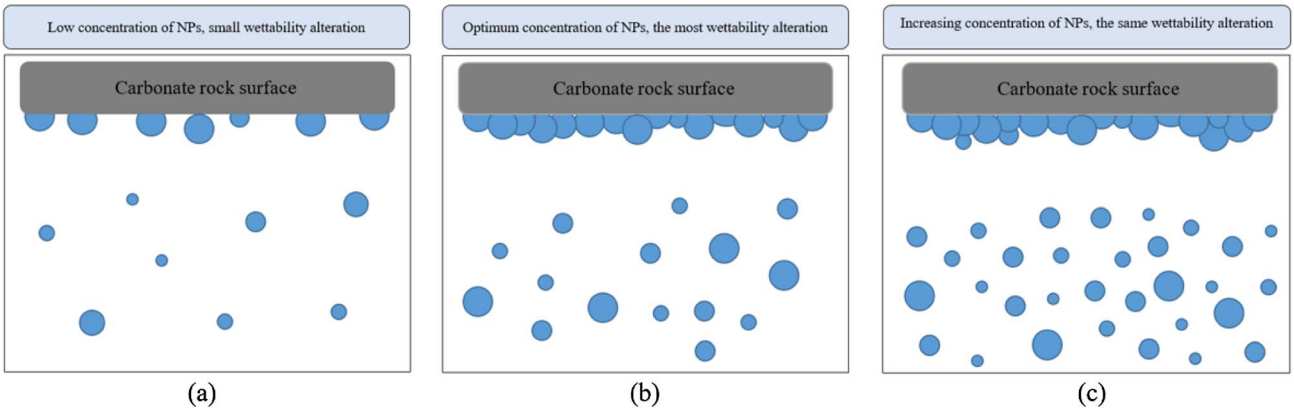

Fig. 13. The effect of an increase in NPs concentration on wettability alteration of carbonate rocks.

cost-effective concentration for wettability alteration. Therefore, concentrations at the second interval sometimes increase the contact angle and, more or less, exacerbates the condition.

3.3 Zeta potential measurements

The electrical charges developed by clay minerals at the solid/solid or solid/fluid interface can lead to a re-arrangement of the charges near the rock surface [31], in a way that neutralization or adsorption of the charges at the interface may happen [54]. Importantly, there is a dependency between contact angle and zeta potential values. In fact, high negative zeta potentials indicate more adsorption of NPs onto the rock surface and thus a higher wettability alteration toward the water-wet condition [55].

Table 5 presents zeta potential measurements for DW and FW + 4 wt.% rock powder, as well as three different nanofluids used in this research. Owing to the positive surface charge of carbonate rocks, the addition of 4 wt.% rock powder to the DW brings a positive zeta potential. This can alter the carbonate surface to the more oil-wet condition

Table 5. Zeta potential measurements of different nanofluids.

Type	Zeta potential (mV)				
	First measurement	Second measurement	Third measurement	Average	Standard deviation
DW + 4 wt.% rock powder	+40.6	+41.9	+42.3	+41.6	0.7
FW + 4 wt.% rock powder	–9.6	–11.1	–10.2	–10.3	0.6
500 ppm nanofluid + 4 wt.% Rock Powder	–40.2	–42.8	–41.4	–41.4	1.0
1000 ppm nanofluid + 4 wt.% rock powder	–48.7	–46.2	–46.0	–46.9	1.2
2000 ppm nanofluid + 4 wt.% rock powder	–32.5	–29.5	–31.1	–31.0	1.2

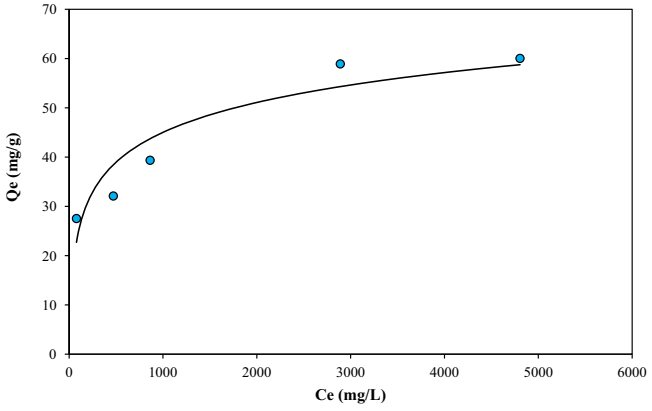

Fig. 14. Amount of adsorbed asphaltene with asphaltene concentration.

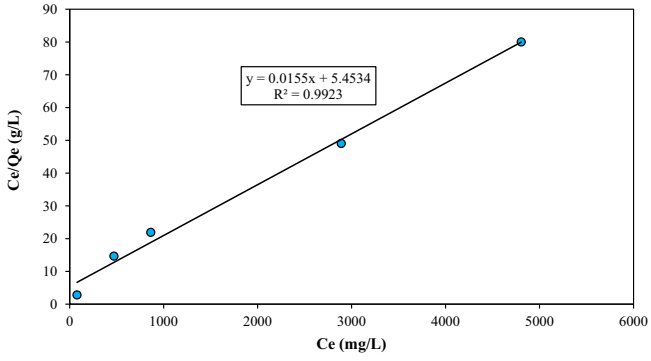

Fig. 15. The diagram of calculation parameters of the Langmuir model.

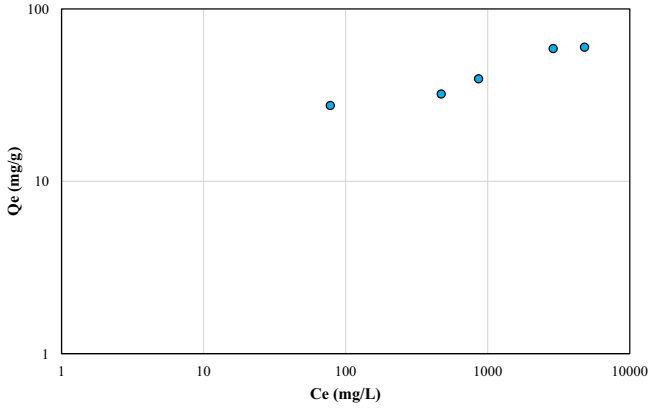

Fig. 16. Q_e *versus* C_e related to the Freundlich model.

due to the adsorption of negative carbocyclic groups present in the crude oil onto the rock surface. With the addition of 4 wt.% rock powder to the FW, potential-determining ions (including but not limited to SO_4^{2-}, Ca^{2+}, Mg^{2+}) present in the FW act as wettability modifier and modify carbonate surface charges. This would result in an inverse zeta potential value from positive (+41.6 mV) to negative (–10.3 mV). However, the results indicate that the wettability alteration by FW is not noticeably high. Adding 500, 1000, and 2000 ppm NPs to the FW + 4 wt.% rock powder supercharge the zeta potential values to –41.4, –46.9, and –31.0, respectively, which implies a strong wettability alteration, as compared to that of FW. The results also are in good accordance with contact angle measurements, in which the fluid included 1000 ppm of NPs was the optimum concentration.

In light of the evidence from previous studies, zeta potential measurements are also good indicators of NPs stability in the base fluid. According to the previous reports, zeta potentials above ±30 mV are in the good stability region [56, 57]. Stable nanofluids are more efficient in the modification of interfacial properties. As it can be seen in Table 5, all nanofluids present a good stability. However, 2000 ppm nanofluid is prone to instability with time, as its zeta potential is on the edge. According to the obtained results, the highest stability belongs to 1000 ppm nanofluid, which is in good agreement with IFT and contact angle results, in which 1000 ppm was the optimum concentration.

3.4 Asphaltene adsorption

There are different adsorption models available for fitting experimental data resulting from batch adsorption

Table 6. Calculated parameters related to the Langmuir and Freundlich Isotherms.

Adsorbent	Temperature (°C)	Langmuir parameters			Freundlich parameters		
		R^2 (–)	Q_m (mg/m^2)	K_L (L/mg)	R^2 (–)	n (–)	K_f (mg/m^2)(L/mg)$^{1/n}$
TiO_2 NPs	25	0.9923	64.52	0.003	0.88	140.84	0.008

experiments. Langmuir and Freundlich models are the most well-known ones adopted in asphaltene adsorption analyses. The former describes a monolayer adsorption, while the latter is associated with the mono/multilayer adsorption. The most important basic assumptions of the Langmuir model are summarized as follows:

- Adsorption ΔH is independent of adsorbed sites and all adsorption sites are equivalent.
- Each adsorption site can only adsorb onto one type of adsorbent.
- Adsorption occurs in a monolayer manner.

Adsorption interactions that follow this model are called "Ideal Adsorption Interactions". In this research, the experimental data were plotted to determine the correct model which best describes the adsorption process and its type of adsorption layer. The Langmuir equation describes monolayer adsorption as follows (eq. (2)):

$$Q_e = Q_m \frac{K_L C_e}{1 + K_L C_e}. \quad (2)$$

In this case, C_e refers to the concentration of asphaltene in toluene/heptane. The terms Q_m and K_L describe the adsorption capacity and adsorption affinity, respectively. In order to obtain the terms K_L and Q_m, the plot of $1/Q_e$ *versus* $1/C_e$ is drawn and the Langmuir constants could be calculated as follows (eq. (3)):

$$\frac{1}{Q_e} = \frac{1}{K_L Q_m C_e} + \frac{1}{Q_m} Q_m = (\text{intercept})^{-1},\ K_L = \frac{\text{intercept}}{\text{slope}} \quad (3)$$

where Q_e is the adsorbed asphaltene (mg/g) and C_e is the asphaltene concentration (mg/L) both at equilibrium. Figure 14 shows the amount of adsorbed asphaltene with asphaltene concentration based on the results obtained from the current analysis.

Figure 15 indicates the plot of C_e/Q_e *versus* C_e for calculation of the Langmuir constants.

Figure 16 depicts the C_e *versus* Q_e related to the Freundlich model, which is used in the determination of Freundlich parameters. Table 6 presents the Langmuir and Freundlich parameters calculated from each plot.

According to the *R*-squared values calculated from plots (Tab. 6), one can conclude that the asphaltene adsorption by TiO_2 NPs is best described by Langmuir Isotherm. Therefore, the adsorption process is a monolayer. This would confirm the role of TiO_2 NPs in the prevention of asphaltene precipitation and deposition, which in turn is effective in the reduction of oil/water IFT and prevention of inducing oil-wet wettability.

4 Conclusion

According to the obtained results, four distinctive groups of results corresponding to IFT, contact angle, zeta potential, and asphaltene adsorption analyses were obtained as follows:

- The oil/water IFT increases with pressure (with or without NPs); however, the presence of TiO_2 NPs in the FW intensifies the increasing rate of IFT with pressure. This effect is due to the increased charge density with pressure increase and therefore the higher aggregation of NPs. What's more, the IFT alterations with pressure in the presence of NPs were found to be different at low and high pressures.
- Temperature has an inverse effect on oil/water IFT values. In fact, as the balance between two phases is established, NPs begin to penetrate relatively from water into the oil phase. As a result, the catalytic behavior of Titania NPs leads to the further reduction of IFT between two phases by thermal cracking of large oil molecules. This thermal cracking varies at different temperatures and, according to the results, is intensified at higher temperatures.
- Altogether, IFT values are different at various pressures, temperatures, as well as different concentrations of NPs in the base fluid. In this research, 1000 ppm TiO_2 nanofluid was found to be the optimum concentration in which the lowest IFT value was attained at 600 psi and 60 °C.
- Based on the obtained results, the initial DW/oil/rock contact angle was 174°, whereas the initial FW/oil/rock contact angle was 161°. The addition of Titania NPs to the FW changed the carbonate rock wettability from strongly oil-wet (174°) to the water-wet condition (34°). The contact angle measurements indicated that two different intervals could be assumed for different concentrations of NPs. At low concentrations (below the optimum concentration), the arrangement of Titania NPs between oil and rock surface induces a disjoining pressure, which overcomes the available oil/solid adhesion force and reduces the contact angles. On the other hand, at high concentrations (beyond optimum concentration), NPs stacking on previous NPs attached to the rock surface does not necessarily reduce the contact angles toward a more water-wet condition.
- Zeta potential measurements revealed that 1000 ppm nanofluid presents the highest stability among all nanofluids, which is, as expected, in good accordance with IFT and contact angle results. In other words, the most stable Titania nanofluid introduced the lowest IFT and contact angle. Therefore, in the

scrutiny of interfacial properties, stability and instability of NPs are of great significance, which can considerably affect the ultimate efficiency. The results also showed that the addition of TiO_2 NPs inverses the zeta potential values from positive to the negative, which confirms the alteration of surface electrical charges for wettability alteration.

- Batch adsorption experiments showed that catalytic TiO_2 NPs presented a monolayer adsorption onto the asphaltene particles since it was best fitted to the Langmuir Isotherm. This would be an asset to the prevention of asphaltene precipitation and deposition, IFT increase, and oil-wet wettability.

References

1 Fakoya M.F., Shah S.N. (2017) Emergence of nanotechnology in the oil and gas industry: Emphasis on the application of silica nanoparticles, *Petroleum* **3**, 4, 391–405.

2 Miranda C.R., Lara L.S.d., Tonetto B.C. (2012) Stability and mobility of functionalized silica nanoparticles for enhanced oil recovery applications, in: *SPE International Oilfield Nanotechnology Conference and Exhibition*, 12–14 June, Noordwijk, The Netherlands, Society of Petroleum Engineers.

3 Sun X., Zhang Y., Chen G., Gai Z. (2017) Application of nanoparticles in enhanced oil recovery: a critical review of recent progress, *Energies* **10**, 3, 345–378.

4 Sun Q., Li Z., Li S., Jiang L., Wang J., Wang P. (2014) Utilization of surfactant-stabilized foam for enhanced oil recovery by adding nanoparticles, *Energy Fuels* **28**, 2384–2394.

5 Kazemzadeh Y., Shojaei S., Riazi M., Sharifi M. (2018b) Review on application of nanoparticles for EOR purposes; a critical of the opportunities and challenges, *Chin. J. Chem. Eng.* DOI: 10.1016/j.cjche.2018.05.022, In press.

6 Rezvani H., Khalilnejad A., Sadeghi-Bagherabadi A.A. (2018) Comparative experimental study of various metal oxide nanoparticles for the wettability alteration of carbonate rocks in EOR processes, in: *80th EAGE Conference and Exhibition 2018*, 11–14 June, Copenhagen, Denmark.

7 Rezvani H., Riazi M., Tabaei M., Kazemzadeh Y., Sharifi M. (2018b) Experimental investigation of interfacial properties in the EOR mechanisms by the novel synthesized Fe_3O_4@ Chitosan nanocomposites, *Colloids Surf. A Physicochem. Eng. Aspects.* **544**, 15–27.

8 Kazemzadeh Y., Eshraghi S.E., Kazemi K., Sourani S., Mehrabi M., Ahmadi Y. (2015a) Behavior of asphaltene adsorption onto the metal oxide nanoparticle surface and its effect on heavy oil recovery, *Ind. Eng. Chem. Res.* **54**, 233–239.

9 Kazemzadeh Y., Eshraghi S.E., Sourani S., Reyhani M. (2015b) An interface-analyzing technique to evaluate the heavy oil swelling in presence of nickel oxide nanoparticles, *J. Mol. Liq.* **211**, 553–559.

10 Kazemzadeh Y., Malayeri M., Riazi M., Parsaei R. (2015c) Impact of Fe_3O_4 nanoparticles on asphaltene precipitation during CO_2 injection, *J. Nat. Gas Sci. Eng.* **22**, 227–234.

11 Kazemzadeh Y., Sharifi M., Riazi M. (2018) Mutual effects of Fe_3O_4/Chitosan nanocomposite and different ions in water for stability of w/o emulsions at low-high salinities, *Energy Fuels* **32**, 12, 12101–12117.

12 Kazemzadeh Y., Sharifi M., Riazi M., Rezvani H., Tabaei M. (2018a) Potential effects of metal oxide/SiO_2 nanocomposites in EOR processes at different pressures, *Colloids Surf. A Physicochem. Eng. Aspects* **559**, 372–384.

13 Kashefi S., Lotfollahi M.N., Shahrabadi A. (2018) Investigation of asphaltene adsorption onto zeolite beta nanoparticles to reduce asphaltene deposition in a silica sand pack, *Oil Gas Sci. Technol. – Rev. IFP Energies nouvelles* **73**, 2.

14 Liao D.L., Liao B.Q. (2007) Shape, size and photocatalytic activity control of TiO_2 nanoparticles with surfactants, *J. Photochem. Photobiol. A Chem.* **187**, 2, 363–369.

15 Xiao X., Ouyang K., Liu R., Liang J. (2009) Anatase type titania nanotube arrays direct fabricated by anodization without annealing, *Appl. Surf. Sci.* **255**, 3659–3663.

16 Dambournet D., Belharouak I., Amine K. (2009) Tailored preparation methods of TiO_2 anatase, rutile, brookite: mechanism of formation and electrochemical properties, *Chem. Mater.* **22**, 3, 1173–1179.

17 Regonini D., Bowen C.R., Jaroenworaluck A., Stevens R. (2013) A review of growth mechanism, structure and crystallinity of anodized TiO2 nanotubes, *Mater. Sci. Eng. R Rep.* **74**, 377–406.

18 Esmaeilzadeh P., Sadeghi M.T., Bahramian A. (2018) Production improvement in gas condensate reservoirs by wettability alteration, using superamphiphobic titanium oxide nanofluid, *Oil Gas Sci. Technol. – Rev. IFP Energies nouvelles* **73**, 46.

19 Bennetzen M.V., Mogensen K. (2014) Novel applications of nanoparticles for future enhanced oil recovery, in: *International Petroleum Technology Conference*, 10–12 December, Kuala Lumpur, Malaysia, International Petroleum Technology Conference.

20 Jiang R., Li K., Horne R. (2017) A mechanism study of wettability and interfacial tension for EOR using silica nanoparticles, in: *SPE Annual Technical Conference and Exhibition*, 9–11 October, San Antonio, Texas, USA, Society of Petroleum Engineers.

21 Sepehrinia K. (2017) Molecular dynamics simulation for surface and transport properties of fluorinated silica nanoparticles in water or decane: Application to gas recovery enhancement, *Oil Gas Sci. Technol. – Rev. IFP Energies nouvelles* **72**, 3, 17.

22 Panahpoori D., Dehdari B., Riazi M., Parsaei R. (2018) Visualization experiments on the impact of surfactant and nanoparticle on EOR potential of foam injection, in: *Innovations in Geosciences – Time for Breakthrough*, 9–12 April, Saint Petersburg, Russia, European Association of Geologists and Engineers.

23 Zhang H., Nikolov A., Wasan D. (2014) Enhanced oil recovery (EOR) using nanoparticle dispersions: Underlying mechanism and imbibition experiments, *Energy Fuels* **28**, 5, 3002–3009.

24 Li K., Wang D., Jiang S. (2018) Review on enhanced oil recovery by nanofluids, *Oil Gas Sci. Technol. – Rev. IFP Energies nouvelles* **73**, 37.

25 Haroun M.R., Alhassan S., Ansari A.A., Al Kindy N.A.M., Abou Sayed N., Kareem A., Ali B., Sarma H.K. (2012) Smart nano-EOR process for Abu Dhabi carbonate reservoirs, in: *Abu Dhabi International Petroleum Conference and Exhibition*, 11–14 November, Abu Dhabi, UAE, Society of Petroleum Engineers.

26 Moghadam T.F., Azizian S. (2014) Effect of ZnO nanoparticles on the interfacial behavior of anionic surfactant at

liquid/liquid interfaces, *Colloids Surf. A Physicochem. Eng. Aspects* **457**, 333–339.
27 Castillo J., Vargas V., Piscitelli V., Ordoñez L., Rojas H. (2017) Study of asphaltene adsorption onto raw surfaces and iron nanoparticles by AFM force spectroscopy, *J. Pet. Sci. Eng.* **151**, 248–253.
28 Franco-Aguirre M., Zabala R.D., Lopera S.H., Franco C.A., Cortés F.B. (2018) Interaction of anionic surfactant-nanoparticles for gas-Wettability alteration of sandstone in tight gas-condensate reservoirs, *J. Nat. Gas Sci. Eng.* **51**, 53–64.
29 Villard J.-M., Buckley J.S., Morrow N.R., Gauchet R. (1993) Wetting and Waterflood Oil Recovery of a Moderately Viscous Crude Oil, in: *Advances in core technologies*, 1993, Texas, Huston, USA, Society of Core Analysts.
30 Rezvani H., Khalilnezhad A., Ganji P., Kazemzadeh Y. (2018a) How ZrO2 nanoparticles improve the oil recovery by affecting the interfacial phenomena in the reservoir conditions?, *J. Mol. Liq.* **252**, 158–168.
31 Rodríguez K., Araujo M. (2006) Temperature and pressure effects on zeta potential values of reservoir minerals, *J. Coll. Interf. Sci.* **300**, 2, 788–794.
32 Zhang P., Tweheyo M.T., Austad T. (2007) Wettability alteration and improved oil recovery by spontaneous imbibition of seawater into chalk: Impact of the potential determining ions Ca^{2+}, Mg^{2+}, and SO_4^{2-}, *Colloids Surf. A Physicochem. Eng. Aspects* **301**, 1, 199–208.
33 Zhang Y., Morrow N.R. (2006) Comparison of secondary and tertiary recovery with change in injection brine composition for crude-oil/sandstone combinations, in: *SPE/DOE symposium on improved oil recovery*, 22–26 April, Tulsa, Oklahoma, USA, Society of Petroleum Engineers.
34 Nassar N.N. (2010) Asphaltene adsorption onto alumina nanoparticles: Kinetics and thermodynamic studies, *Energy Fuels* **24**, 8, 4116–4122.
35 Hosseinpour N., Khodadadi A.A., Bahramian A., Mortazavi Y. (2013) Asphaltene adsorption onto acidic/basic metal oxide nanoparticles toward in situ upgrading of reservoir oils by nanotechnology, *Langmuir* **29**, 14135–14146.
36 Ye Z., Zhang F., Han L., Luo P., Yang J., Chen H. (2008) The effect of temperature on the interfacial tension between crude oil and gemini surfactant solution, *Colloids Surf. A Physicochem. Eng. Aspects* **322**, 138–141.
37 Jennings H.Y. (1967) The effect of temperature and pressure on the interfacial tension of benzene-water and normal decane-water, *J. Coll. Interf. Sci.* **24**, 3, 323–329.
38 Tang G.-Q., Kovscek A. (2004) An experimental investigation of the effect of temperature on recovery of heavy oil from diatomite, *SPE J.* **9**, 2, 163–179.
39 Hjelmeland O., Larrondo L. (1986) Experimental investigation of the effects of temperature, pressure, and crude oil composition on interfacial properties, *SPE Res. Eng.* **1**, 4, 321–328.
40 Moeini F., Hemmati-Sarapardeh A., Ghazanfari M.-H., Masihi M., Ayatollahi S. (2014) Toward mechanistic understanding of heavy crude oil/brine interfacial tension: The roles of salinity, temperature and pressure, *Fluid Phase Equilib.* **375**, 191–200.
41 Cai B.-Y., Yang J.-T., Guo T.-M. (1996) Interfacial tension of hydrocarbon + water/brine systems under high pressure, *J. Chem. Eng. Data* **41**, 3, 493–496.
42 Manshad A.K., Olad M., Taghipour S.A., Nowrouzi I., Mohammadi A.H. (2016) Effects of water soluble ions on interfacial tension (IFT) between oil and brine in smart and carbonated smart water injection process in oil reservoirs, *J. Mol. Liq.* **223**, 987–993.
43 Flock D., Le T., Gibeau J. (1986) The effect of temperature on the interfacial tension of heavy crude oils using the pendent drop apparatus, *J. Can. Pet. Technol.* **25**, 02.
44 Lashkarbolooki M., Ayatollahi S., Riazi M. (2014) The impacts of aqueous ions on interfacial tension and wettability of an asphaltenic–acidic crude oil reservoir during smart water injection, *J. Chem. Eng. Data* **59**, 11, 3624–3634.
45 Hashemi R., Nassar N.N., Pereira-Almao P. (2012) Transport behavior of multimetallic ultradispersed nanoparticles in an oil-sands-packed bed column at a high temperature and pressure, *Energy Fuels* **26**, 3, 1645–1655.
46 Mohammadi M., Akbari M., Fakhroueian Z., Bahramian A., Azin R., Arya S. (2011) Inhibition of asphaltene precipitation by TiO_2, SiO_2, and ZrO_2 nanofluids, *Energy Fuels* **25**, 3150–3156.
47 Vorkapic D., Matsoukas T. (1998) Effect of temperature and alcohols in the preparation of titania nanoparticles from alkoxides, *J. Am. Ceram. Soc.* **81**, 11, 2815–2820.
48 Xuan Y., Li Q., Hu W. (2003) Aggregation structure and thermal conductivity of nanofluids, *AIChE J.* **49**, 4, 1038–1043.
49 Roustaei A., Moghadasi J., Bagherzadeh H., Shahrabadi A. (2012) An experimental investigation of polysilicon nanoparticles' recovery efficiencies through changes in interfacial tension and wettability alteration, in: *SPE International Oilfield Nanotechnology Conference and Exhibition*, 12–14 June, Noordwijk, The Netherlands, Society of Petroleum Engineers.
50 Ogolo N., Olafuyi O., Onyekonwu M. (2012) Enhanced oil recovery using nanoparticles, in: *SPE Saudi Arabia Section Technical Symposium and Exhibition*, 8–11 April, Al-Khobar, Saudi Arabia, Society of Petroleum Engineers.
51 ShamsiJazeyi H., Miller C.A., Wong M.S., Tour J.M., Verduzco R. (2014) Polymer-coated nanoparticles for enhanced oil recover, *J. Appl. Polym. Sci.* **131**, 15, 15–28.
52 Nassar N.N., Hassan A., Vitale G. (2014) Comparing kinetics and mechanism of adsorption and thermo-oxidative decomposition of Athabasca asphaltenes onto TiO_2, ZrO_2, and CeO_2 nanoparticles, *Appl. Catal. A Gen.* **484**, 161–171.
53 Tian H., Wang M. (2018) Electrokinetic mechanism of wettability alternation at oil-water-rock interface, *Surf. Sci. Rep.* **72**, 369–391.
54 Srinivasan S. (2006) *Fuel cells: From fundamentals to applications*, Springer Science & Business Media, Berlin, Germany.
55 Taqvi S.T., Almansoori A., Bassioni G. (2016) Understanding the role of Asphaltene in wettability alteration using ζ potential measurements, *Energy Fuels* **30**, 3, 1927–1932.
56 O'Brien R.W. (1990) Electroacoustic studies of moderately concentrated colloidal suspensions, *Faraday Disc. Chem. Soc.* **90**, 301–312.
57 Hanaor D., Michelazzi M., Leonelli C., Sorrell C.C. (2012) The effects of carboxylic acids on the aqueous dispersion and electrophoretic deposition of ZrO_2, *J. Eur. Ceram. Soc.* **32**, 235–244.